

Mirror, mirror: Landau-Zener-Stückelberg-Majorana interferometry of a superconducting qubit in front of a mirror

P. Y. Wen,¹ O. V. Ivakhnenko,^{2,3} M. A. Nakonechnyi,² B. Suri,⁴ J.-J. Lin,¹ W.-J. Lin,⁵ J. C. Chen,¹ S. N. Shevchenko,^{2,3,6,*} Franco Nori,^{3,7} and I.-C. Hoi^{1,8,†}

¹*Department of Physics, National Tsing Hua University, Hsinchu 30013, Taiwan*

²*B. Verkin Institute for Low Temperature Physics and Engineering, Kharkov 61103, Ukraine*

³*Theoretical Quantum Physics Laboratory, Cluster for Pioneering Research, RIKEN, Wako-shi, Saitama 351-0198, Japan*

⁴*Department of Instrumentation and Applied Physics,*

Indian Institute of Science, Bengaluru 560012, India

⁵*Department of Physics, National Taiwan University, Taipei 10617, Taiwan*

⁶*V. N. Karazin Kharkiv National University, Kharkov 61022, Ukraine*

⁷*Department of Physics, The University of Michigan, Ann Arbor, MI 48109-1040, USA*

⁸*Center for Quantum Technology, National Tsing Hua University, Hsinchu 30013, Taiwan*

(Dated: December 17, 2024)

We investigate the Landau-Zener-Stückelberg-Majorana interferometry of a superconducting qubit in a semi-infinite transmission line terminated by a mirror. The transmon-type qubit is at the node of the resonant electromagnetic (EM) field, “hiding” from the EM field. “Mirror, mirror” briefly describes this system, because the qubit acts as another mirror. We modulate the resonant frequency of the qubit by applying a sinusoidal flux pump. We probe the spectroscopy by measuring the reflection coefficient of a weak probe in the system. Remarkable interference patterns emerge in the spectrum, which can be interpreted as multi-photon resonances in the dressed qubit. Our calculations agree well with the experiments.

PACS numbers: 42.50.Gy, 85.25.Cp

I. INTRODUCTION

In recent years, superconducting artificial atoms¹ coupled to open transmission-line waveguide have been a fast growing field, called waveguide Quantum Electrodynamics (w-QED), which provides a unique platform to investigate atom-light interaction. The uniqueness of w-QED, as compared to conventional cavity QED, is that atoms are coupled to continuum modes of the electromagnetic (EM) field in the waveguide. Exciting problems in w-QED include: resonance fluorescence of an artificial atom², photon-mediated interactions between distant artificial atoms³, atom in front of a mirror⁴, time dynamics in atom-like mirrors⁵, photon routing⁶, generation of non-classical microwaves⁷, cross-Kerr effect⁸, amplification without population inversion⁹, collective Lamb shift between two distant artificial atoms¹⁰, ultra strong coupling¹¹, quantum rifling¹², probabilistic motional averaging¹³.

When a two-level system is driven back and forth around its resonance frequency, it will produce Landau-Zener-Stückelberg-Majorana (LZSM) interference. LZSM interferometry^{14–16} has been studied in atomic systems¹⁷, quantum dots¹⁸, charge and spin qubits^{19,20} and superconducting qubit in cavity^{21–24}, among others. However, the effect of LZSM has not been explored with a single artificial atom in front of a mirror, where the artificial atom is coupled to a continuum of modes of the EM field in the transmission-line waveguide, and the atom interferes with its mirror image, as in Refs. [4,25].

LZSM interferometry is important for both system de-

scription and control²⁶. However, for this to be realized, one needs to have the avoided energy-level crossing in the spectrum as a function of a controlling parameter. One example of systems without this are transmon-type superconducting qubits, where the energy levels are almost independent of the bias voltage. The way to cure this was studied in Ref. [27], which studied the qubit by chirping the microwave frequency, which results in dressed states with avoided-level crossing. In this work, we study a transmon qubit driven by two fields (see also Ref. [28]). One of these dresses the qubit and creates the spectrum with the avoided-level crossing, while the other one makes the system periodically pass around the avoided-level point. This allows to study LZSM interferometry in a qubit placed in front of a mirror. “Mirror, mirror” briefly describes this system, because the qubit acts as another mirror.

II. SUPERCONDUCTING QUBIT IN FRONT OF A MIRROR

In this work, we investigate the LZSM interferometry of a superconducting qubit in a semi-infinite transmission line, at a distance terminated by a mirror. In particular, the qubit is located at the node of the resonant EM field, where it is hiding from the EM field. We then modulate the resonant frequency of the qubit by applying a sinusoidal wave through an on-chip flux pump. In addition, the coupling between the EM field and qubit is also being modulated. We then probe the spectroscopy of the system by applying a weak probe field along the

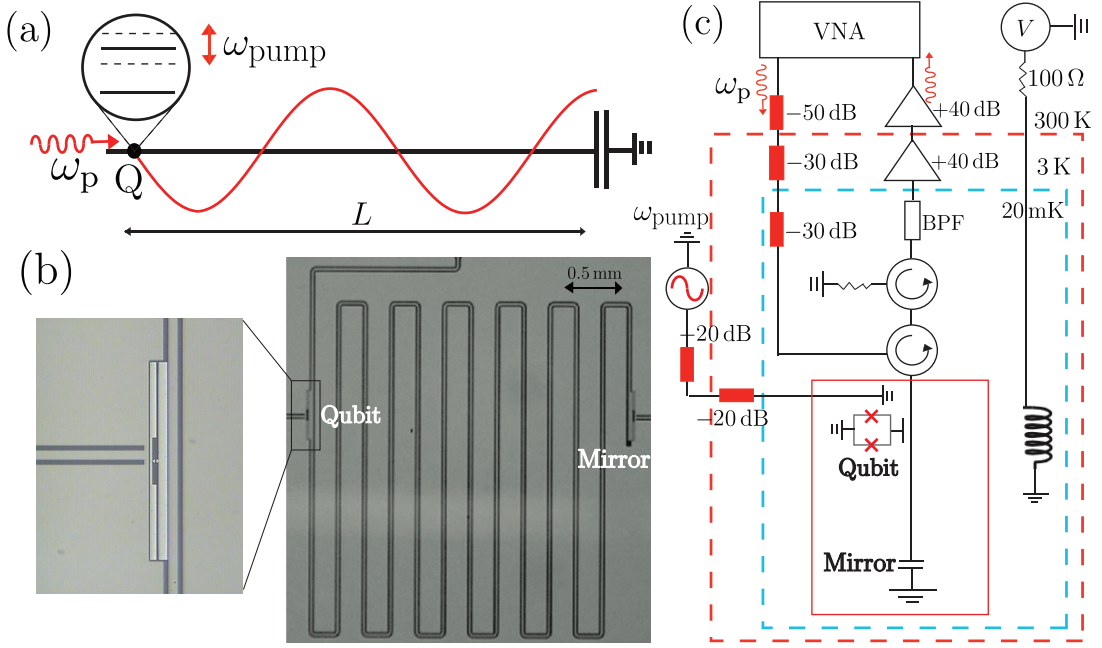


Figure 1: The experimental setup and device (a) A conceptual sketch of the device showing the electromagnetic mode (red curve) in the transmission line. The qubit is located at the node of the resonant mode of the EM field, hiding from the EM field. The qubit is subjected to a sinusoidal drive along the transmission line with frequency ω_p , and a flux pump ω_{pump} . (b) A photo of the device. The qubit (shown in the zoom-in on the left; the two long bright parts form the qubit capacitance and the gap in the middle between them is bridged by two Josephson junctions forming a SQUID loop) is placed $L \simeq 33$ mm from another qubit, which sits at the end of the transmission line (i.e., at the mirror). Note that the qubit at the end of the transmission line is not in use in this work, because it is far detuned. The characteristic impedance of the transmission line is $Z_0 \simeq 50 \Omega$. By tuning the qubit transition frequency $\omega_{10}(\Phi)$, we tune the qubit to the node of the EM field. (c) A sketch of the setup for the experiment. The qubit frequency can be tuned by a global magnetic field from a superconducting coil controlled by V . For measurements, a coherent signal at frequency ω_p is generated by a vector network analyzer (VNA) at room temperature and fed through attenuators (red squares) to the sample, which sits in a cryostat cooled at 20 mK to avoid thermal fluctuations affecting the experiment. The reflected signal passes a bandpass filter (BPF) and amplifiers, and is then measured with the VNA. Here ω_{pump} is the flux pump to modulate the transition frequency of the qubit.

transmission line and measure the reflection coefficient. Interesting interference patterns emerge in the spectrum, which can be explained by multi-photon resonances in the dressed qubit. New features appear, as compared to conventional LZSM interference; for example, now the zero-order Rabi sideband vanishes (see also Ref. [29]).

Figure 1 shows (a) a sketch of the device, (b) the image of the device, and (c) the measurement setup. A transmon qubit^{30–32} is embedded in a semi-1D transmission line with characteristic impedance $Z_0 \simeq 50 \Omega$, with the ground (excited) state $|0\rangle$ ($|1\rangle$). The $|0\rangle \leftrightarrow |1\rangle$ transition energy is $\hbar\omega_{10}(\Phi) \approx \sqrt{8E_J(\Phi)E_C} - E_C$, which is determined by the single-electron charging energy $E_C = e^2/2C_\Sigma$, where C_Σ is the total capacitance of the qubit, and the flux-dependent Josephson energy $E_J(\Phi) = E_{J,\text{max}}|\cos(\pi\Phi/\Phi_0)|$; $\Phi_0 = h/2e$ is the magnetic flux quantum. The E_C determines the anharmonicity of the qubit.

In Fig. 1(c), a probe field of frequency ω_p is fed into the transmission line. The pump field of frequency ω_{pump} is applied to the on-chip flux line, sinusoidally modulating the transition frequency of the qubit. The key parameters

Value	Description	Range
ω_{10}	qubit frequency, $\omega_{10} = \omega_{10}(V)$	$\simeq \omega_{\text{node}}$
δ	pump amplitude; $\delta = \delta(P_{\text{pump}})$	$\sim 0.1 \text{ GHz} \cdot 2\pi$
ω_{pump}	pump frequency	$< 0.1 \text{ GHz} \cdot 2\pi$
ω_p	probe frequency	$\simeq \omega_{\text{node}}$

Table I: Table of controllable parameters. Here $\omega_{\text{node}} = 4.75 \text{ GHz} \cdot 2\pi$.

are summarized in Table I.

III. THEORETICAL DESCRIPTION

Let us now consider the qubit Hamiltonian, with details presented in Appendix A. Thanks to the mirror, the transmission-line voltage at the point of coupling the qubit, $x = L$, is proportional to $\cos(\omega_p L/v)$. When this factor is zero, this gives the node frequency ω_{node} , with $\cos(\omega_{\text{node}} L/v) = 0$. For small offset, $\Delta\omega = \omega_p - \omega_{\text{node}} \ll \omega_p$, instead of $\cos(\omega_p L/v)$, we have $\Delta\omega/\omega_{\text{node}}$, which shows that at $\Delta\omega = 0$ the qubit is “hidden” or “decou-

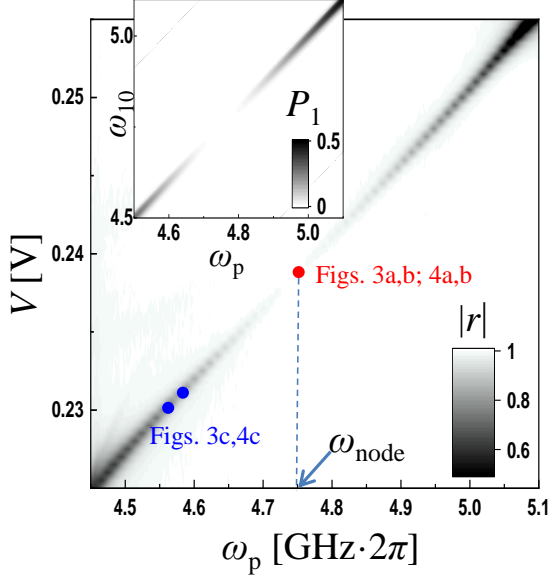


Figure 2: Amplitude of the reflection coefficient $|r|$ for a weak coherent probe as a function of probe frequency ω_p and qubit frequency ω_{10} (controlled by the voltage V). The spectroscopy shows how the response disappears when the qubit ends up at a node for the EM field around $\omega_p = \omega_{\text{node}} \simeq 4.75 \text{ GHz} \cdot 2\pi$, denoted by the dashed line marker. The red dot indicates the qubit bias point in Fig. 3a,b and Fig. 4a,b. The blue dots correspond to the qubit bias point in Fig. 3c and Fig. 4c, respectively. The details of the flux dependence can be seen in Ref. [10]. Inset shows the calculated qubit upper-level occupation probability P_1 as a function of the probe frequency ω_p and the qubit frequency ω_{01} (both in $\text{GHz} \cdot 2\pi$), where $\omega_{10} \propto V$.

pled” from the transmission line. So, we have the Hamiltonian

$$H = -\frac{B_z}{2}\sigma_z - \frac{B_x}{2}\sigma_x, \quad (1)$$

of which the diagonal part is the energy-level modulation

$$B_z/\hbar = \omega_{10} + \delta \sin \omega_{\text{pump}} t, \quad (2)$$

and the off-diagonal part describes the coupling to the probe signal

$$B_x/\hbar = G \sin \omega_p t. \quad (3)$$

Importantly, here the coupling constant G is proportional to the frequency offset $\Delta\omega$,

$$G = G_0 \frac{\Delta\omega}{\omega_{\text{node}}}, \quad (4)$$

and G_0 is proportional to the probe signal amplitude.

The observable value is the reflection coefficient r , namely its deviation from 1. The impact of the qubit is in suppressing r . Thus, following Refs. [21,22,26], we associate the reflection coefficient to the qubit upper-level occupation probability P_1 . From the stationary solution

of the Bloch equations, for this value we have (see e.g. Refs. [19,33]):

$$P_1 = \frac{1}{2} \sum_{k=-\infty}^{\infty} \frac{G_k^2}{G_k^2 + [(\omega_p - \omega_{10}) - k\omega_{\text{pump}}]^2 \frac{\Gamma_1}{\Gamma_2} + \Gamma_1 \Gamma_2}, \quad (5)$$

where the renormalized driving amplitude $G_k = G J_k(\delta/\omega_{\text{pump}})$ follows the oscillating Bessel function J_k of the first kind; Γ_1 and $\Gamma_2 = \Gamma_1/2 + \Gamma_\phi$ are the relaxation and decoherence rates with the pure dephasing rate Γ_ϕ being much smaller than Γ_1 . With this formula, Eq. (5), we plot theoretical graphs in Figs. 2, 3, and 4. For this we use $G_0 = 0.1 \text{ GHz} \cdot 2\pi$, $\Gamma_1 < 40 \text{ MHz} \cdot 2\pi$, $\Gamma_2 \approx \Gamma_1/2$ (i.e. $\Gamma_\phi \ll \Gamma_1$).

IV. MEASUREMENTS

We first perform single-tone spectroscopy of the qubit-mirror system. In Fig. 2, the resonant frequency of the qubit is tuned by voltage. As the voltage increases, the linewidth of the qubit decreases from a finite linewidth to zero, and then increases back to a finite linewidth. At the frequency where the linewidth vanishes, around $\omega_{10} = \omega_{\text{node}} \simeq 4.75 \text{ GHz} \cdot 2\pi$, the qubit is located at the node of the EM field, as indicated by the vertical dashed line, where it is hiding from the EM field.

By using two-tone spectroscopy¹⁰, we know that $E_C/\hbar \simeq 324 \text{ MHz}$. For $\omega_{10}/2\pi = 4.75 \text{ GHz}$, the corresponding Josephson energy is $E_J/\hbar \simeq 9.9 \text{ GHz}$.

After the basic characterization of the system, we want to study the spectrum as a function of the following parameters: qubit frequency ω_{10} , pump amplitude δ , pump frequency ω_{pump} , and probe frequency ω_p . For spectroscopy, we always use a weak probe amplitude in experiments.

To start with, we set the qubit frequency corresponding to the node as a working point, where $\omega_{10} = \omega_{\text{node}}$. We then apply a sinusoidal flux pump at a fixed power to the qubit, and sweep the pump frequency from 1 MHz to 100 MHz. At the same time, we probe the spectroscopy of the system using a weak field ω_p near the qubit frequency. We show the amplitude reflection coefficient $|r|$ in Fig. 3(a,b) as a function of ω_{pump} and ω_p in (a) for $P_{\text{pump}} = -45 \text{ dBm}$, in (b) for $P_{\text{pump}} = -38 \text{ dBm}$. We observed LZSM interference fringes. These interference fringes can be interpreted as multi-photon resonances in the dressed qubit. Multi-photon resonances appear at $\omega_p = \omega_{10} \pm k\omega_{\text{pump}}$, where k is the order, as indicated in the figures. The zero order, where $k = 0$, is missing, which is a key feature here, different from conventional LZSM interference fringes. In Fig. 3(b), we can clearly see the order k up to ± 4 . We increase the pump power in Fig. 3 from -45 dBm in (a) to -38 dBm in (b), and the gap between negative k and positive k fringes becomes wider. Indeed, the stronger the pump power, the wider they separate (data not shown). The power in Fig. 3 (a)

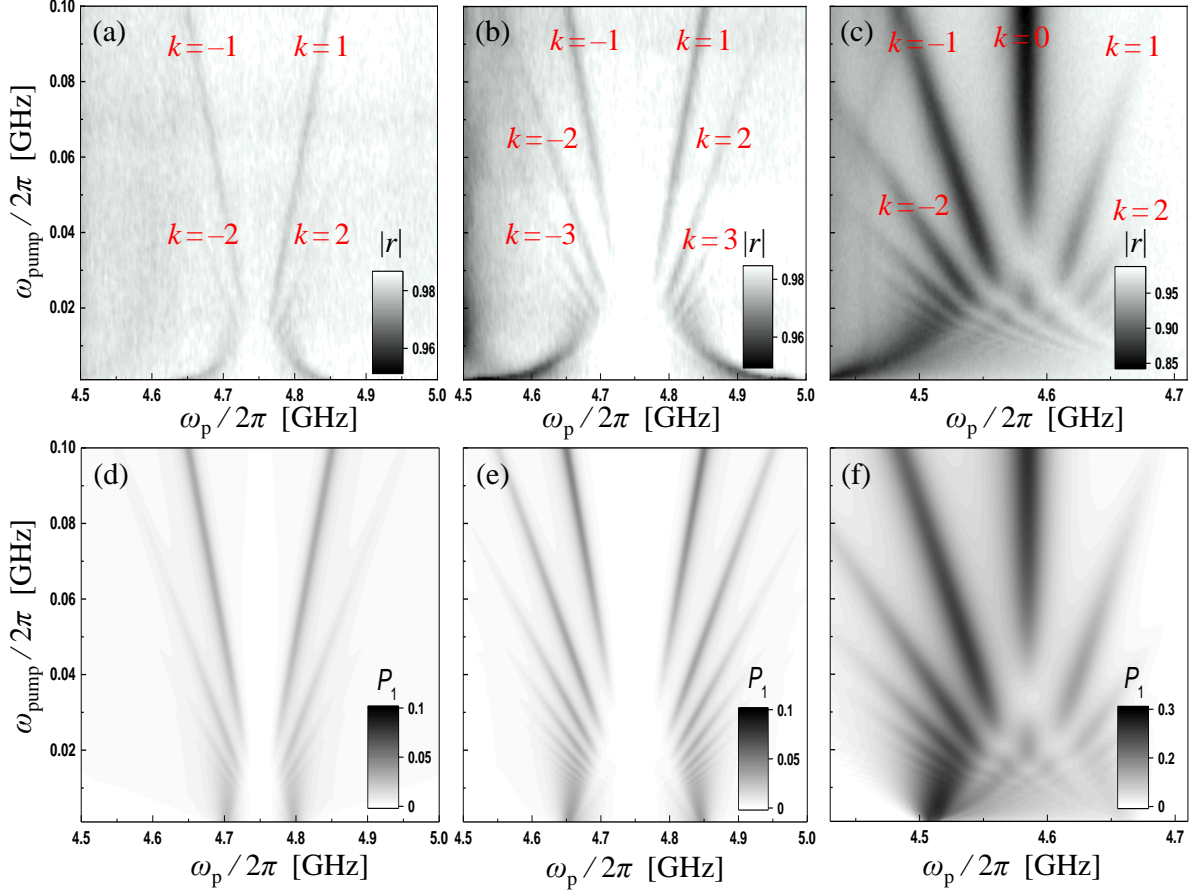


Figure 3: Sinusoidal modulation of the qubit by flux pumping with the resonance frequency at a fixed pump power P_{pump} . Amplitude reflection coefficient $|r|$ for a weak coherent probe as a function of the probe frequency ω_p and pump frequency ω_{pump} ; (a,b,c) are experimental data, while (d,e,f) are our theoretical calculations. (a) Qubit biased at $\omega_{\text{node}} = 4.75 \text{ GHz} \cdot 2\pi$, the flux pump power is fixed at $P_{\text{pump}} = -45 \text{ dBm}$. (b) Qubit biased at the node around 4.75 GHz with $P_{\text{pump}} = -38 \text{ dBm}$. (c) Qubit biased at 4.58 GHz , red detuned from the node, and $P_{\text{pump}} = -38 \text{ dBm}$. Note that the k -dependent multi-photon resonances emerge: $\Delta\omega = k\omega_{\text{pump}}$. In (b), we can see Rabi sidebands at k from -4 to 4 . In (a) and (b), the $k = 0$ Rabi sideband disappears whereas in (c) the $k = 0$ Rabi sideband appears. For (a) and (b), the positive k and negative k fringes are symmetric, whereas, in (c) the interference fringes are not symmetric along $k = 0$. As the fringes approach the node regime, near 4.75 GHz , they become weaker. In (d-f) we show the respective calculated qubit upper-level occupation probabilities P_1 .

and (b) differs by 7 dB, meaning that their pump amplitude δ , differ by a factor of 2.2. This is also what happens in the theory calculation plots. In this sense, this separation can be used to calibrate the pump power. In Fig. 3(c), we bias the qubit at around 4.58 GHz , red detuned from the node, and we then see asymmetric interference fringes. At this bias point, when the qubit is pumped in the negative part of the sinusoidal, the qubit is pumped toward the larger linewidth regime, see Fig. 2. However, when the qubit is pumped in the positive part of the sinusoidal, the qubit is pumped towards the zero-linewidth regime; therefore, we can see that the interference fringes vanish near ω_{node} . In addition, as compared to (a) and (b), the $k = 0$, zero Rabi sideband appears in (c).

Next, we keep the pump frequency ω_{pump} constant. We change the power of the pump P_{pump} from -70 dBm to

-30 dBm , and probe the system with a weak field near the resonance frequency of the qubit. In Fig. 4, we show in (a) and (b) $\omega_{\text{pump}}/2\pi = 10 \text{ MHz}$ and 100 MHz for the qubit frequency at node ω_{node} , and $\omega_{\text{pump}}/2\pi = 10 \text{ MHz}$ for the qubit frequency red detuned from ω_{node} in (c). These plots show the amplitude reflection coefficient $|r|$ as a function of the probe frequency ω_p and the pump power P_{pump} . In Fig. 4(a,b), when the flux pump is weak (this corresponds to a small change of the qubit resonance frequency) there are no interference fringes in the interference pattern, as indicated in (a) and (b). This can be explained using Fig. 2, where the “node regime” corresponds to 4.7 GHz to 4.8 GHz , and there is no response for a weak flux pump. When the pump power increases, this corresponds to larger changes of the resonance frequency, we see the Rabi-splitting-like behavior in (a). In (b), Rabi sidebands at $k = -2, -1, +1, +2$

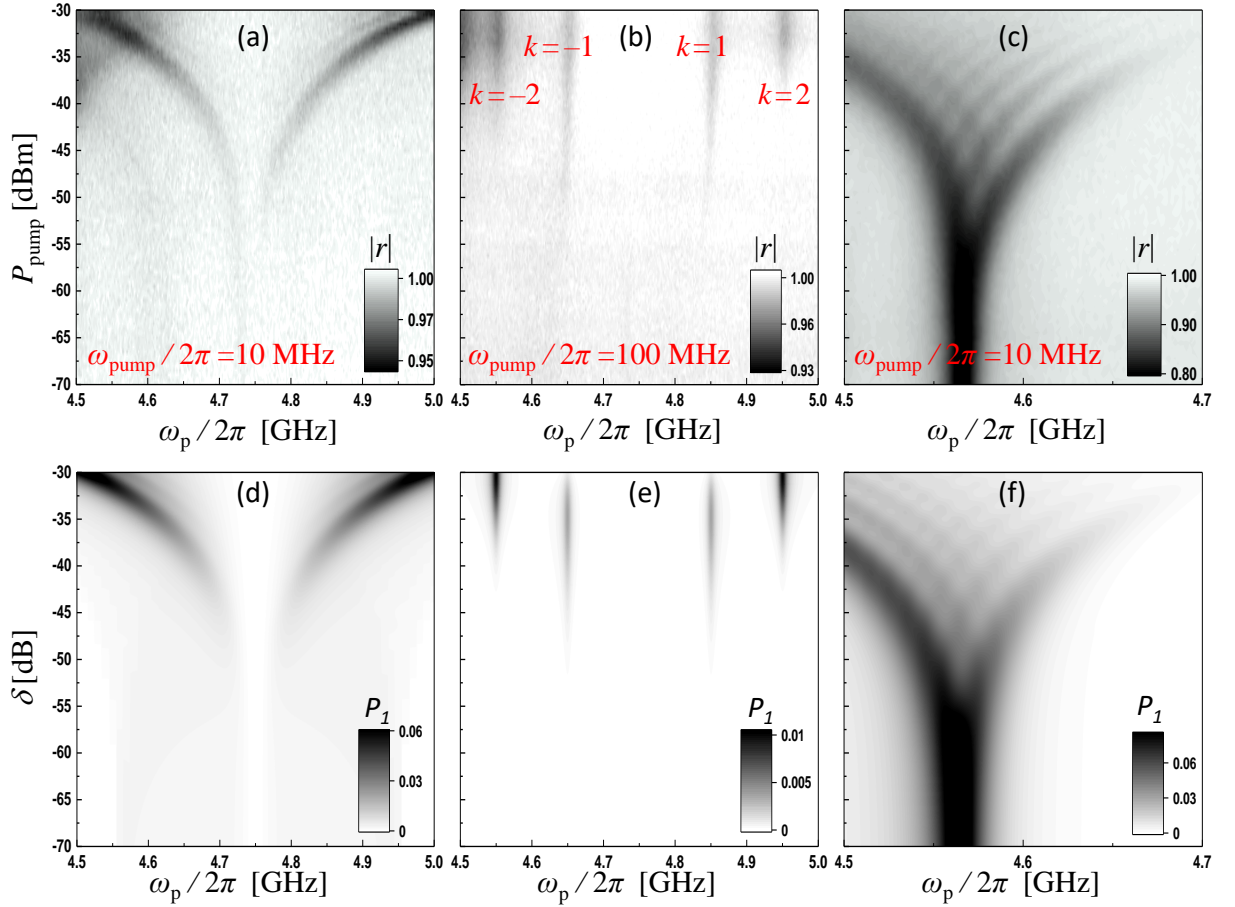


Figure 4: Sinusoidal modulation of the qubit by flux pumping at the resonance frequency at a fixed pump frequency ω_{pump} . The plots show the amplitude of the reflection coefficient $|r|$ for a weak coherent probe versus the probe frequency ω_p and pump power P_{pump} . (a,b,c) correspond to experiments and (d,e,f) to theory. (a) and (b) are at the node around 4.75 GHz with $\omega_{\text{pump}}/2\pi = 10$ MHz and 100 MHz, respectively. Note the Rabi sidebands at $\Delta\omega = k\omega_{\text{pump}}$, with $k = -2, -1, +1, +2$. The higher the pump power, the more resolved sidebands are visible. Note the onset of the Rabi sidebands for $k = \pm 1$ and $k = \pm 2$, for -45 dBm and -35 dBm, respectively. (c) red detuned from the node at 4.56 GHz. In (a,c), we observe Rabi-like splittings as the pump power increases. In (a), we see a symmetric splitting, whereas in (c) there are several asymmetric splittings. In (c), as the fringes approach ω_{node} , they become weaker. In (d-f) we show the respective calculated qubit upper-level occupation probabilities P_1 .

appear. These match the condition $\Delta\omega = k\omega_{\text{pump}}$. The higher the pump power, the more resolved the sideband k becomes. In Fig. 4(c), when we bias the qubit frequency away from ω_{node} , the interference fringes become weaker as the probe frequency approaches the node frequency at 4.75 GHz.

V. CONCLUSIONS

In conclusion, we investigate the LZSM interferometry of a superconducting qubit in a semi-infinite transmission line terminated by a mirror. When the qubit frequency is set to the node of the EM field, after flux pumping the qubit frequency, remarkable interference patterns emerge, which can be interpreted as multi-photon resonances in the dressed qubit. We see multi-photon reso-

nances up to 4th order. The zero-order photon resonance disappears. One of the advantages of this atom-mirror arrangement is that we can effectively manipulate the absorption properties of the two-level atom, providing a novel way to manipulate the quantum states.

Acknowledgments

I.-C.H. and J.C.C. would like to thank I. A. Yu and C.-Y. Mou for fruitful discussions. This work was financially supported by the Center for Quantum Technology from the Featured Areas Research Center Program within the framework of the Higher Education Sprout Project by the Ministry of Education (MOE) in Taiwan. I.-C.H. acknowledges financial support from the MOST of Taiwan under project 109-2636-M-007-007. J.C.C. ac-

knowledges financial support from the MOST of Taiwan under project 107-2112-M-007-003-MY3. O.V.I., M.A.N., and S.N.S. acknowledge partial support by the Grant of the President of Ukraine (Grant No. F84/185-2019). F.N. is supported in part by the MURI Center for Dynamic Magneto-Optics via the Air Force Office of Scientific Research (AFOSR) (FA9550-14-1-0040), Army Research Office (ARO) (Grant No. Grant No. W911NF-18-1-0358), Japan Science and Technology Agency (JST) (via the Q-LEAP program, and the CREST Grant No. JPMJCR1676), Japan Society for the Promotion of Science (JSPS) (JSPS-RFBR Grant No. 17-52-50023, and JSPS-FWO Grant No. VS.059.18N), the RIKEN-AIST Challenge Research Fund, the Foundational Questions Institute (FQXi), and the NTT PHI Laboratory.

Appendix A: Hamiltonian

In this Appendix we describe how we obtain the Hamiltonian (1) for a qubit in front of a mirror, schematically shown in Fig. 5.

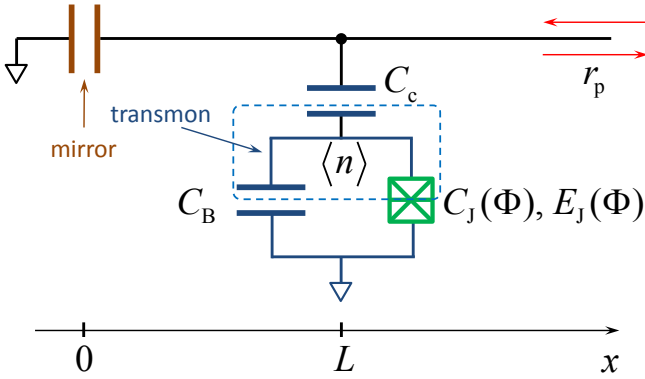


Figure 5: Schematic diagram of a capacitively shunted charge qubit in front of a mirror. The qubit and the transmission line are coupled through the capacitance C_c . The transmission line is biased by a probe signal and its reflection coefficient r_p is measured. The line is terminated by a capacitor, playing the role of a mirror. The transmon qubit consists of Josephson junctions, described by the flux-dependent capacitance $C_J(\Phi)$, shunted by a capacitance C_B .

The transmission line is described by the voltage $V(x, t)$ and current $I(x, t)$:

$$V(x, t) = V(x)e^{i\omega_p t}, \quad I(x, t) = I(x)e^{i\omega_p t}, \quad (\text{A1})$$

with

$$V(x) = V_+ e^{ikx} + V_- e^{-ikx}, \quad (\text{A2})$$

$$I(x) = -\frac{V_+}{Z_0} e^{ikx} + \frac{V_-}{Z_0} e^{-ikx}, \quad (\text{A3})$$

where $k = \omega_p/v$. Thanks to the mirror at $x = 0$, we

have $I(0) = 0$, $V_- = V_+$, and $V(x) = 2V_+ \cos(kx)$ for $x \in (0, L)$.

The transmon is described by the number of Cooper pairs on it $\langle n \rangle$, with the number operator given by the Pauli matrix³⁴

$$n = \left(\frac{E_J}{32E_C} \right)^{1/4} \sigma_x. \quad (\text{A4})$$

If we take here $\hbar\omega_{10} \approx \sqrt{8E_C E_J}$, we have

$$n = \sqrt{\frac{\hbar\omega_{10}}{E_C}} \sigma_x. \quad (\text{A5})$$

Then, writing down the charges of the respective capacitor plates, we obtain the island voltage³⁵

$$V_I = \frac{2e}{C_\Sigma} \langle n \rangle - \frac{C_c}{C_\Sigma} V(L, t), \quad (\text{A6})$$

where $C_\Sigma = C_J + C_B + C_c$. With this we can write the Hamiltonian of the transmon qubit coupled to the transmission line, which can be rewritten (omitting c-numbers) as follows

$$\begin{aligned} H_c &= \frac{1}{2} C_c [V(L, t) - V_I]^2 \rightarrow C_c V(L, t) V_I \rightarrow \\ &\rightarrow eV_+ \frac{C_c}{C_\Sigma} \sqrt{\frac{\hbar\omega_{10}}{E_C}} \cos\left(\frac{\omega_p L}{v}\right) \sin(\omega_p t) \sigma_x. \end{aligned} \quad (\text{A7})$$

For a small frequency offset, $\Delta\omega = \omega_p - \omega_{\text{node}} \ll \omega_p$, we have

$$\cos\left(\frac{\omega_p L}{v}\right) \approx \frac{\pi}{2} \frac{\Delta\omega}{\omega_{\text{node}}}, \quad (\text{A8})$$

with $\cos(\omega_{\text{node}} L/v) = 0$. Then the Hamiltonian (A7) describes the off-diagonal part of the transmon Hamiltonian (1) with

$$\begin{aligned} G &= G_0 \frac{\Delta\omega}{\omega_{\text{node}}}, \\ G_0(V_+) &= \frac{\pi}{\hbar} \frac{C_c}{C_\Sigma} \sqrt{\frac{\hbar\omega_{10}}{E_C}} eV_+. \end{aligned} \quad (\text{A9})$$

This is written in the main text as Eq. (3).

Consider next the diagonal part of the transmon Hamiltonian given by the energy-level splitting

$$\hbar\omega_{10} = \sqrt{8E_C E_J(\Phi)} - E_C. \quad (\text{A10})$$

The flux contains the dc and ac components, $\Phi = \Phi_{\text{dc}} + \Phi_{\text{ac}} \sin(\omega_{\text{pump}} t)$. Assuming the latter being a small value, we obtain

$$\hbar\omega_{10} = \hbar\omega_{10}(\Phi_{\text{dc}}) + \hbar\delta(\Phi_{\text{ac}}) \sin(\omega_{\text{pump}} t), \quad (\text{A11})$$

where $\delta(\Phi_{\text{ac}}) \propto \Phi_{\text{ac}}$ is the driving amplitude. This is written in the main text as Eq. (2).

- * e-mail: sshevchenko@ilt.kharkov.ua
† e-mail: ichoi@phys.nthu.edu.tw
- ¹ X. Gu, A. F. Kockum, A. Miranowicz, Y.-X. Liu, and F. Nori, “Microwave photonics with superconducting quantum circuits,” *Phys. Rep.* **718-719**, 1–102 (2017).
 - ² O. Astafiev, A. M. Zagoskin, A. A. Abdumalikov, Y. A. Pashkin, T. Yamamoto, K. Inomata, Y. Nakamura, and J. S. Tsai, “Resonance fluorescence of a single artificial atom,” *Science* **327**, 840–843 (2010).
 - ³ K. Lalumiere, B. C. Sanders, A. F. van Loo, A. Fedorov, A. Wallraff, and A. Blais, “Input-output theory for waveguide QED with an ensemble of inhomogeneous atoms,” *Phys. Rev. A* **88**, 043806 (2013).
 - ⁴ I.-C. Hoi, A. F. Kockum, L. Tornberg, A. Pourkabirian, G. Johansson, P. Delsing, and C. M. Wilson, “Probing the quantum vacuum with an artificial atom in front of a mirror,” *Nat. Phys.* **11**, 1045–1049 (2015).
 - ⁵ M. Mirhosseini, E. Kim, X. Zhang, A. Sipahigil, P. B. Dieterle, A. J. Keller, A. Asenjo-Garcia, D. E. Chang, and O. Painter, “Cavity quantum electrodynamics with atomlike mirrors,” *Nature* **569**, 692 (2019).
 - ⁶ I.-C. Hoi, C. M. Wilson, G. Johansson, T. Palomaki, B. Peropadre, and P. Delsing, “Demonstration of a single-photon router in the microwave regime,” *Phys. Rev. Lett.* **107**, 073601 (2011).
 - ⁷ I.-C. Hoi, T. Palomaki, J. Lindkvist, G. Johansson, P. Delsing, and C. M. Wilson, “Generation of nonclassical microwave states using an artificial atom in 1D open space,” *Phys. Rev. Lett.* **108**, 263601 (2012).
 - ⁸ I.-C. Hoi, A. F. Kockum, T. Palomaki, T. M. Stace, B. Fan, L. Tornberg, S. R. Sathyamoorthy, G. Johansson, P. Delsing, and C. M. Wilson, “Giant Cross-Kerr effect for propagating microwaves induced by an artificial atom,” *Phys. Rev. Lett.* **111**, 053601 (2013).
 - ⁹ P. Y. Wen, A. F. Kockum, H. Ian, J. C. Chen, F. Nori, and I.-C. Hoi, “Reflective amplification without population inversion from a strongly driven superconducting qubit,” *Phys. Rev. Lett.* **120**, 053601 (2018).
 - ¹⁰ P. Y. Wen, K.-T. Lin, A. F. Kockum, B. Suri, H. Ian, J. C. Chen, S. Y. Mao, C. C. Chiu, P. Delsing, F. Nori, G.-D. Lin, and I.-C. Hoi, “Large collective Lamb shift of two distant superconducting artificial atoms,” *Phys. Rev. Lett.* **123**, 233602 (2019).
 - ¹¹ P. Forn-Diaz, J. J. Garcia-Ripoll, B. Peropadre, J.-L. Orgiazzi, M. A. Yurtalan, R. Belyansky, C. M. Wilson, and A. Lupascu, “Ultrastrong coupling of a single artificial atom to an electromagnetic continuum in the nonperturbative regime,” *Nat. Phys.* **13**, 39–43 (2017).
 - ¹² D. Szombati, A. Gomez Friero, C. Müller, T. Jones, M. Jerger, and A. Fedorov, “Quantum rifling: Protecting a qubit from measurement back action,” *Phys. Rev. Lett.* **124**, 070401 (2020).
 - ¹³ D. S. Karpov, V. Y. Monarkha, D. Szombati, A. G. Friero, A. N. Omelyanchouk, E. Il’ichev, A. Fedorov, and S. N. Shevchenko, “Probabilistic motional averaging,” *arXiv:1912.04557* (2019).
 - ¹⁴ W. D. Oliver, Y. Yu, J. C. Lee, K. K. Berggren, L. S. Levitov, and T. P. Orlando, “Mach-Zehnder interferometry in a strongly driven superconducting qubit,” *Science* **310**, 1653–1657 (2005).
 - ¹⁵ M. Sillanpää, T. Lehtinen, A. Paila, Y. Makhlin, and P. Hakonen, “Continuous-time monitoring of Landau-Zener interference in a Cooper-pair box,” *Phys. Rev. Lett.* **96**, 187002 (2006).
 - ¹⁶ S. N. Shevchenko, S. Ashhab, and F. Nori, “Landau-Zener-Stückelberg interferometry,” *Phys. Rep.* **492**, 1–30 (2010).
 - ¹⁷ C. S. E. van Ditzhuijzen, A. Tauschinsky, and H. B. van Linden van den Heuvell, “Observation of Stückelberg oscillations in dipole-dipole interactions,” *Phys. Rev. A* **80**, 063407 (2009).
 - ¹⁸ A. Bogan, S. Studenikin, M. Korkusinski, and L. Gaudreau, “Landau-Zener-Stückelberg-Majorana interferometry of a single hole,” *Phys. Rev. Lett.* **120**, 207701 (2018).
 - ¹⁹ K. Ono, S. N. Shevchenko, T. Mori, S. Moriyama, and F. Nori, “Quantum interferometry with a g -factor-tunable spin qubit,” *Phys. Rev. Lett.* **122**, 207703 (2019).
 - ²⁰ R. M. Otxoa, A. Chatterjee, S. N. Shevchenko, S. Barraud, F. Nori, and M. F. Gonzalez-Zalba, “Quantum interference capacitor based on double-passage Landau-Zener-Stückelberg-Majorana interferometry,” *Phys. Rev. B* **100**, 205425 (2019).
 - ²¹ J. Li, M. P. Silveri, K. S. Kumar, J.-M. Pirkkalainen, A. Vepsäläinen, W. C. Chien, J. Tuorila, M. A. Sillanpää, P. J. Hakonen, E. V. Thuneberg, and G. S. Paraoanu, “Motional averaging in a superconducting qubit,” *Nat. Comm.* **4**, 1420 (2013).
 - ²² M. Silveri, K. Kumar, J. Tuorila, J. Li, A. Vepsäläinen, E. Thuneberg, and G. Paraoanu, “Stueckelberg interference in a superconducting qubit under periodic latching modulation,” *New J. Phys.* **17**, 043058 (2015).
 - ²³ J. Pan, Y. Fan, Y. Li, X. Dai, X. Wei, Y. Lu, C. Cao, L. Kang, W. Xu, J. Chen, G. Sun, and P. Wu, “Dynamically modulated Autler-Townes effect in a transmon qubit,” *Phys. Rev. B* **96**, 024502 (2017).
 - ²⁴ T. Bera, S. Majumder, S. K. Sahu, and V. Singh, “Large flux-mediated coupling in hybrid electromechanical system with a transmon qubit,” *arXiv:2001.05700*.
 - ²⁵ J. Eschner, C. Raab, F. Schmidt-Kaler, and R. Blatt, “Light interference from single atoms and their mirror images,” *Nature* **413**, 495 (2001).
 - ²⁶ T. Wu, Y. Zhou, Y. Xu, S. Liu, and J. Li, “Landau-Zener-Stückelberg interference in nonlinear regime,” *Chin. Phys. Lett.* **36**, 124204 (2019).
 - ²⁷ M. Gong, Y. Zhou, D. Lan, Y. Fan, J. Pan, H. Yu, J. Chen, G. Sun, Y. Yu, S. Han, and P. Wu, “Landau-Zener-Stückelberg-Majorana interference in a 3D transmon driven by a chirped microwave,” *Applied Phys. Lett.* **108**, 112602 (2016).
 - ²⁸ A. M. Satanin, M. V. Denisenko, A. I. Gelman, and F. Nori, “Amplitude and phase effects in Josephson qubits driven by a biharmonic electromagnetic field,” *Phys. Rev. B* **90**, 104516 (2014).
 - ²⁹ G. Giavaras and Y. Tokura, “in preparation,” (2020).
 - ³⁰ J. Q. You, J. S. Tsai, and F. Nori, “Hybridized solid-state qubit in the charge-flux regime,” *Phys. Rev. B* **73**, 014510 (2006).
 - ³¹ J. Q. You, X. Hu, S. Ashhab, and F. Nori, “Low-decoherence flux qubit,” *Phys. Rev. B* **75**, 140515 (2007).
 - ³² A. F. Kockum and F. Nori, “Quantum Bits with Josephson Junctions,” in *Fundamentals and Frontiers of the Josephson Effect* (Springer International Publishing, 2019) pp.

- 703–741.
- ³³ O. V. Ivakhnenko, S. N. Shevchenko, and F. Nori, “Simulating quantum dynamical phenomena using classical oscillators: Landau-Zener-Stückelberg-Majorana interferometry, latching modulation, and motional averaging,” *Sci. Rep.* **8**, 12218 (2018).
- ³⁴ J. Koch, T. M. Yu, J. Gambetta, A. A. Houck, D. I. Schuster, J. Majer, A. Blais, M. H. Devoret, S. M. Girvin, and R. J. Schoelkopf, “Charge-insensitive qubit design derived from the Cooper pair box,” *Phys. Rev. A* **76**, 042319 (2007).
- ³⁵ S. N. Shevchenko and D. S. Karpov, “Thermometry and memcapacitance with qubit-resonator system,” *Phys. Rev. Applied* **10**, 014013 (2018).